Advanced Journal of Chemistry, Section A

Journal homepage: www.ajchem-a.com

Original Research Article

One-Pot Microwave-Assisted Synthesis of Chlorinated Benzylamine-Substituted Pyrazine Derivatives and *In Silico* Studies of Their Potential as EGFR and HER2 Inhibitors

Widiastuti Agustina Eko Setyowati*, Imarotul Unsiyah, Celicarina Anwar, Muhammad Hizbul Wathon, Elfi Susanti VH, Sri Retno Dwi Ariani

Department of Chemistry Education, Faculty of Teacher Training and Education, Universitas Sebelas Maret, Surakarta, Indonesia

ARTICLEINFO

Article history

Submitted: 2025-12-14
Revised: 2026-01-24
Accepted: 2026-02-09
ID: AJCA-2512-2000
DOI: 10.48309/AJCA.2026.565862.2000

KEYWORDS

Pyrazine
Chlorinated benzylamine
Microwave-assisted synthesis
Molecular docking

ABSTRACT

Pyrazine is widely used in pharmaceuticals, and benzylamine offers advantages due to its reactive amine group, while the chloro-substituent may enhance its metabolic stability. This suggests that the structural modification of pyrazines using chlorinated benzylamine may provide novel molecules with enhanced biological activity; however, such modifications have not been extensively pursued. This study aims to synthesize chlorinated benzylamine-substituted pyrazine derivatives, obtain an effective synthetic method, and determine their potential as EGFR and HER2 inhibitors. Synthesis was carried out using three methods, namely microwave-assisted synthesis (MAS), ultrasound-assisted synthesis (UAS), and conventional methods. Three benzylamine-substituted pyrazine derivatives, namely 3-amino-*N*-(3-chlorobenzyl)pyrazine-2-carboxamide (**1**), 3-amino-*N*-(4-chlorobenzyl)pyrazine-2-carboxamide (**2**), and 3-amino-*N*-(2,4-dichlorobenzyl)pyrazine-2-carboxamide (**3**), have been successfully synthesized. The structures of compounds **1**-**3** have been determined comprehensively based on FT-IR, ^{1}H- NMR, ^{13}C-NMR, HMBC, HSQC, and HRMS spectra. MAS proved to be superior, performing the synthesis in a much faster time (30 min), with higher yields (78-93%) compared to UAS (61-69%) and conventional methods (58-65%). Compound **1** is predicted to be more favorable as an EGFR inhibitor, while compound **3** is more favorable as an HER2 inhibitor. Predicted pharmacokinetics, toxicity, and drug-likeness of compounds **1**-**3** provide a good initial safety prediction, but experimental toxicology is necessary to confirm the safety issues. These three compounds are recommended for further *in vitro* and *in vivo* studies as EGFR and HER2 inhibitors.

* Corresponding author: Setyowati, Widiastuti Agustina Eko
✉ E-mail: widiastuti_aes@staff.uns.ac.id

GRAPHICAL ABSTRACT

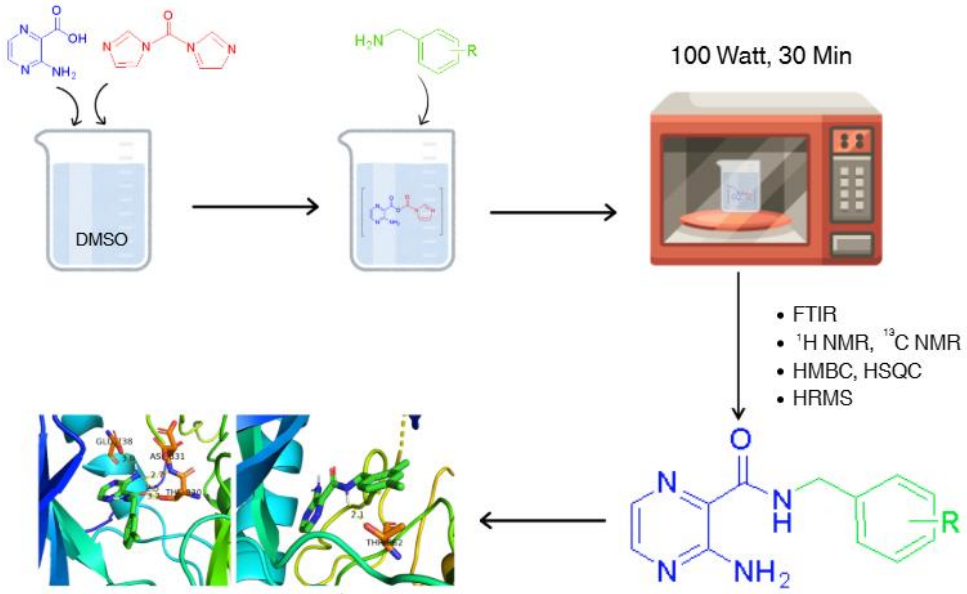

Introduction

Pyrazine is a privileged scaffold widely used in the design of bioactive ligands. The presence of two nitrogen atoms in the aromatic ring allows pyrazine to interact stably with key residues on enzymatic targets and receptors, thus enhancing its potential in the development of new drug candidates. Comprehensive pharmacological analyses in recent years have shown that various pyrazine derivatives possess broad biological activities, including antibacterial, anti-inflammatory, and anticancer activities [1,2].

In vitro and *in silico* studies have shown that substitutions in the pyrazine ring can increase ligand affinity for the active domains of various protein kinases that play a role in cell proliferation. Several studies have reported the ability of pyrazine derivatives to suppress cancer cell growth through apoptosis induction, cell cycle modulation, and inhibition of tyrosine kinase-mediated pro-survival signaling pathways [3,4]

Two important targets that have become a primary focus in the development of kinase-based cancer therapies are the epidermal growth factor receptor (EGFR) and human epidermal growth factor receptor 2 (HER2). Both receptors play a role in the tumorigenesis of various cancers, including lung, breast, and ovarian cancers. Although several clinical inhibitors are available, such as gefitinib, erlotinib, and lapatinib, the emergence of mutational resistance and issues with pharmacological selectivity remain significant obstacles to the development of advanced therapies. Molecular design-based approaches using pyrazine derivatives represent a novel strategy for basic screening to generate more selective inhibitors for EGFR and HER2.

Pyrazine structural modifications have been widely used to enhance their biological activity [2], including through nitration, acetylation, esterification, bromination, and amidation reactions [5,6]. Aromatic substitution modifications and the insertion of electron-withdrawing groups can increase the inhibitory potency against both EGFR and HER2 and improve the ADME profile of drug candidates [7]. One compound that can be considered for modifying the pyrazine structure is benzylamine. Studies have shown that the presence of an amine group adjacent to the benzyl ring facilitates favorable orientation into the ligand back pocket

and allows H-bond formation with surface residues or solvents. The addition of chlorine to the benzyl ring can offer several advantages. Structurally, the chlorine atom can be involved in halogen bonding or hydrophobic interactions that place the aromatic ring in an optimal position in the kinase affinity pocket. Therefore, chlorinated benzylamines have the potential to enhance the affinity and ADME profiles of candidate inhibitors when paired with a pyrazine core [8–10].

The synthesis of novel compounds combining pyrazine structures with chlorinated benzylamines has the potential to produce compounds with broader biological activity properties, but research on this subject has not been widely conducted. In this study, the synthesis of chlorinated benzylamine-substituted pyrazine derivatives was carried out using conventional methods, UAS, and MAS. This research expands on the previous study [11], which synthesized pyrazine derivatives using only conventional methods. The use of UAS and MAS in this study is a novel. The synthesis was conducted in a one-pot system. This study describes a more effective and efficient method for synthesizing chlorinated benzylamine-substituted pyrazine derivatives. In addition, a molecular docking study was conducted to predict the interaction between ligands and protein targets [12]. The *in silico* study was also complemented by ADME/Tox profiles as a basic screening to predict the potential of these compounds as selective cancer drug candidates for EGFR and HER2.

Experimental

Materials and methods

The general procedure for the synthesis of pyrazine derivatives was carried out according to the method [12] with slight modifications. 3-Aminopyrazine-2-carboxylic acid (1 eq) was dissolved in DMSO, and then carbonyldiimidazole (CDI) (2 eq) was added and left at room temperature for 10 minutes. The resulting solution was added to 3 eq benzylamine derivatives (3-chlorobenzylamine, 4-chlorobenzylamine, 2,4-dichlorobenzylamine) then heated. In the conventional methods, the reaction was carried out for 4 hours at 100 °C. UAS was conducted at room temperature for 2 hours, while the MAS was carried out at 100 watts (60 °C) for 30 minutes. The reaction was monitored by thin layer chromatography (TLC) using n-hexane: ethyl acetate = 2: 1 and visualized with a UV-Vis detector at λ=254 nm.

The molecular structure was determined based on FT-IR, NMR, and HRMS data. NMR measurements were performed in 1D and 2D using Varian Unity INOVA Agilent Technologies at 25 °C. 1D NMR measurements were performed to determine the number and type of protons (^{1}H 500 MHz) and carbon (^{13}C 125 MHz). 2D NMR measurements were performed to determine the proton-carbon single bond correlation (HSQC) and the correlation between carbon and protons separated by two, three, and four bonds (HMBC). The molecular mass of the synthesized product was determined using high-resolution mass spectroscopy Waters LCT Premier XE ESI-TOF HRMS.

Molecular docking was performed using AutoDock Vina 1.5.6 [13,14] and the results were visualized using BIOVIA Discovery Studio 2024 Client [15,16], and PyMOL 1.3 Delano Scientific LLC, Italy [17]. The target proteins used were EGFR (PDB ID: 1M17) [18] and HER2 (PDB ID: 3PP0) [19], obtained from the Protein Data Bank. Pharmacokinetic predictions were run through SwissADME and toxicity predictions using ProTox-II.

*3-Amino-N-(3-chlorobenzyl)pyrazine-2-carboxamide (**1**)*

White solid. ^{1}H-NMR (500 MHz, DMSO): 9.38 (*t*, 1H, *J*= 6.35), 8.22 (*d*, 1H, *J*= 2.3), 7.84 (*d*, 1H, *J*= 2.3), 7.52 (*bs*, 2H), 7.36 (*t*, 1H, *J*= 2.0), 7.28 (*t*, 2H, *J*= 7.9),

7.33 (*d*, 1H, *J*= 7.7), and 4.44 (*d*, 2H, *J*= 6.4). ^{13}C-NMR (125 MHz, DMSO): 166.2, 155.2, 147.0, 142.2, 132.9, 131.0, 130.2, 127.2, 126.1, 125.6, and 41.7. HRESITOF-MS (positive mode) *m/z* $[M+H]^+$ 263.0693 *(m/z* $[M + H]^+$ calculation for $C_{12}H_{12}N_4OCl$ 263.0700). NMR, and HRMS data of **1** are provided in Supplementary Information.

*3-Amino-N-(4-chlorobenzyl)pyrazine-2-carboxamide (**2**)*

White solid. ^{1}H-NMR (500 MHz, DMSO): 9.36 (*t*, 1H, *J*= 6.35), 8.21(*d*, 1H, *J*= 2,35), 7.83 (*d*, 1H, *J*= 2,3), 7.54 (bs, 2H), 7.35 (*dd*, 4H, *J*= 8.7, 20.6), and 4.42 (*d*, 2H, *J*= 6,4). ^{13}C-NMR (125 MHz, DMSO): 166.1, 155.2, 146.9, 138.6, 131.3, 131.0, 129.2, 128.2, 125.6, and 41.5. HRESITOF-MS (positive mode) *m/z* $[M+H]^+$ 247.0991 *(m/z* $[M + H]^+$ calculation for $C_{12}H_{12}N_4OCl$ 263.0700). NMR and HRMS data of **2** are demonstrated in Supplementary Information.

*3-Amino-N-(2,4-dichlorobenzyl)pyrazine-2-carboxamide (**3**)*

White solid. ^{1}H-NMR (500 MHz, DMSO): 9.34 (*t*, 1H, *J*= 6.35), 8.24 (*d*, 1H, *J*= 2,35), 7.86 (*d*, 1H, *J*= 2,3), 7.60 (*d,* 1H, *J*= 2.1), 7.48 (*bs*, 2H), 7.39 (*dd,* 1H, *J*= 8.35; 2,1), 7.30 (*d*, 1H, *J*= 8,35), and 4.49 (*d*, 2H, *J*= 6,25). ^{13}C-NMR (125 MHz, DMSO): 166.3, 155.2, 147.2, 135.6, 132.7, 132.1, 131.1, 129.7, 128.5, 127.4, 125.4, and 60.5. HRESITOF-MS (positive mode) m/z $[M+H]^+$ 297.0309 (m/z $[M + H]^+$ calculation for $C_{12}H_{10}N_4OCl_2$ 297.0310). NMR and HRMS data of **3** are indicated Supplementary Information.

Results and Discussion

The synthesis of chlorinated benzylamine-substituted pyrazine derivatives was carried out by reacting 3-aminopyrazine-2-carboxylic acid as a starting material with three chlorinated benzylamine derivatives (3-chlorobenzylamine, 4-chlorobenzylamine, and 2,4-dichlorobenzylamine) using 1,1'-carbonyldiimidazole (CDI) as a coupling agent in anhydrous dimethyl sulfoxide (DMSO) [20]. This reaction took place in one pot with two steps. The first step of CDI functions to activate the carboxylic acid, changing the acidic –OH group, which is a less favorable leaving group into a good leaving group. The reaction between 3-aminopyrazine-2-carboxylic acid and CDI forms the intermediate (3-aminopyrazine-2-yl)(1*H*-imidazol-1-yl)methanone. In the second step, the intermediate will react with chlorinated benzylamine derivatives to form compounds **1**, **2**, and **3** (Figure 1) [12,21]. The intermediate resulting from CDI activation (1st step) is formed directly in the reaction system without isolation/purification in the previous stage and reacts directly with the benzylamine derivative (2nd step) [22].

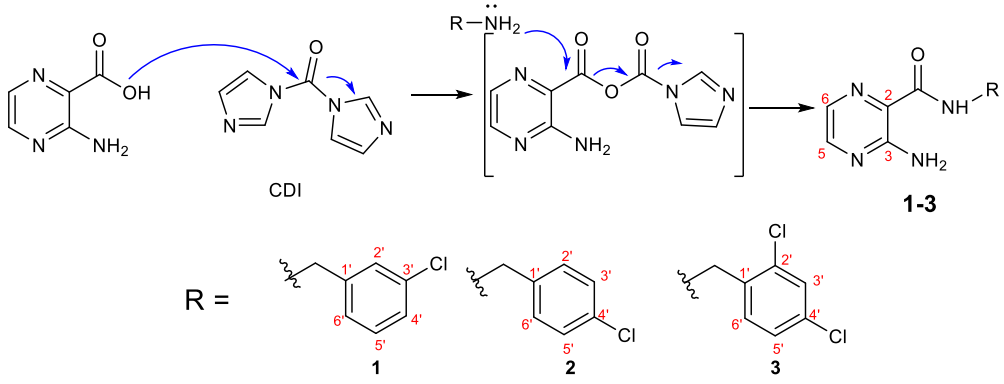

Figure 1. Formation of compounds **1–3**

Figure 1 shows that the starting material contains both carboxylic and amine groups, and both can react with CDI. The carboxylic group reacts much more dominantly with CDI than the amine group present in the starting material. This is because CDI reacts primarily with groups that have nucleophilic oxygen on the carboxylate to form *N*-acylimidazole. This carboxylic activation occurs more quickly and has more favorable kinetics than the direct reaction of CDI with the amine group under normal conditions [23]. Although nitrogen has a lower electronegativity than oxygen, its ability to attack (nucleophilicity) is less reactive due to several obstacles. Nitrogen atoms have greater ionization energy compared to oxygen, making it more difficult for nitrogen to form cations or radicals (N^+ or $N^\bullet$) without the assistance of a photocatalyst or an external electron donor. In amide compounds, the lone electron pair on nitrogen is delocalized in the π system, so it cannot attack the electrophilic center. The electron pair on nitrogen is delocalized toward the carbonyl group, thereby reducing the electron density on nitrogen in heteroaromatic systems, making it less electrophilic. Furthermore, delocalization stabilizes nitrogen but weakens its ability to attack, as the free electron pair is no longer localized, making nitrogen unable to attack [24].

Table 1. Yield of compounds **1–3** by conventional, UAS and MAS methods

Entry	Yield (%) [a]		
	conventional[b]	UAS[c]	MAS[d]
1	65.86	69.19	92.29
2	59.66	61.54	78.67
3	58.76	68.03	93.32

[a] Yield of isolated products; [b] Reflux, 100 °C, 4 h; c Room Temp., 2 h; d 100 watt (60 °C), 30 min.

The synthesis used a substrate: catalyst: reactant ratio of 1: 2: 3 equivalents. The use of CDI is at least 2 equivalents to ensure that all carboxylate groups on the substrate can be fully activated into acyl imidazole intermediates that are reactive to nucleophiles. The appearance of byproducts such as urea is not due to excessive use of CDI but because CDI reacts in humid conditions (presence of water) and at high temperatures [25]. The conventional method successfully produced the target compound, but it required a longer time and a lower yield (59-65%) (Table 1). This was due to the uneven distribution of heat generated by the conventional method.

Synthesis using the UAS method was carried out at room temperature for 2 hours. The synthesis yield was higher (61-69%) than the conventional method (Table 1). The UAS method exhibits a cavitation effect that accelerates the reaction, increases mass transfer efficiency, and reduces energy requirements [26,27].

Synthesis using microwave irradiation achieved higher yields (72–92%) (Table 1). The yield of MAS increased by 25–35% compared to conventional methods and 20–30% compared to UAS. Furthermore, MAS required significantly less time. MAS only requires 30 minutes, which is about 8 times faster than the conventional method (4 hours) and 4 times faster than UAS (2 hours) (Table 1). In terms of energy, MAS operates at 100 W and 60 °C for 30 minutes (Table 1), resulting in lower energy requirements compared to conventional (100 °C, 4 hours). Although UAS is performed at room temperature without external heating, the combination of a much shorter reaction time and higher yield makes MAS more operationally efficient. The use of microwaves allows for very fast reaction rates. The direct interaction between electromagnetic waves and reactant molecules generates internal heat without the need for conduction through the medium [28-32] . Dielectric heating in MAS allows for more direct energy transfer to the reactants, thereby accelerating the reaction and increasing process efficiency [33].

This enables a significant reduction in synthesis time without compromising product purity. Furthermore, the implementation of one-pot

synthesis also reduces intermediate purification, thus saving solvents and generating less waste [28].

The optimization was carried out to determine the MAS optimum reaction conditions for compounds **1**, **2**, and **3**. The optimization carried out included the ratio of substrate to reactant, catalyst (CDI) usage, and reaction time. From the optimization, the optimum conditions for compound **1** were obtained at a substrate to reactant ratio of 1:1 with the use of 3 eq CDI for 30 minutes (Table 2), compound 2 at a substrate to reactant ratio of 1:2.5 with the use of 1 eq CDI catalyst for 30 minutes (Table 3), and compound 3 at a substrate to reactant ratio of 1:2.5 with the use of 2 eq CDI for 30 minutes (Table 4).

Table 2. Microwave-assisted synthesis optimization of compound **1**

Substrate : Reactant (eq)	CDI (eq)	Time (minutes)	Yield (%)
1:3	1	30	48.91
1:3	2	30	70.17
1:3	3	30	72.29
1:1	**3**	30	92.29
1:1.5	3	30	78.29
1:2	3	30	89.84
1:2.5	3	30	79.74
1:3	3	20	63.81
1:3	3	40	48.16

Table 3. Microwave-assisted synthesis optimization of compound **2**

Substrate : Reactant (eq)	CDI (eq)	Time (minutes)	Yield (%)
1:3	1	30	70.17
1:3	2	30	54.75
1:3	3	30	69.11
1:1	1	30	57.25
1:1.5	1	30	30.30
1:2	1	30	70.17
1:2.5	**1**	30	78.67
1:2.5	1	20	30.30
1:2.5	1	40	43.59

Table 4. Microwave-assisted synthesis optimization of compound **3**

Substrate : Reactant (eq)	CDI (eq)	Time (minutes)	Yield (%)
1:3	1	30	73.15
1:3	2	30	77.38
1:3	3	30	71.75
1:1	2	30	66.50
1:1.5	2	30	58.15
1:2	2	30	74.48
1:2.5	2	30	93.32
1:2.5	2	20	41.27
1:2.5	2	40	36.58

The FT-IR spectrum shows a difference in absorption between 3-aminopyrazine-2-carboxylic acid as a substrate or starting material and the product (**1–3**). In the substrate, the absorption of carboxylic acid carbonyl was found at 1,718.65 cm^{-1} followed by the absorption of the hydroxyl group at 3,328.31 cm^{-1}. In compounds **1–3**, the carbonyl absorption shifted towards 1,645 – 1,671 cm^{-1}, which is the absorption of the amide carbonyl, while the absorption of the hydroxyl group was not found. This indicates that the carboxylic group of the substrate has reacted with the amine group of the benzylamine derivative to form a new amide group. The appearance of methylene absorption (1,430 – 1,437 cm^{-1}) in the spectrum of compounds **1–3** strengthens the evidence that the product contains a benzylamine framework (Figure 2). Typical N–H absorption bands were found at 3,146–3,392 cm^{-1}, and C–N amine bands at 1,000-1,300 cm^{-1}. The presence of overlapping bands, especially in the 3,200–3,500 cm^{-1} (N–H/O–H stretching) and 1,000–1,300 cm^{-1} (C–N stretching), occurs because several vibrational modes can appear simultaneously. This type of overlap is generally caused by hydrogen bonds and polar functional groups [34]. Minor band shifts and broadening are also seen due to the influence of the solvent environment and intermolecular interactions, especially for the amide C=O and N–H vibrations. FT-IR data are interpreted as supporting evidence, with structural confirmation dependent on NMR and HRMS analysis (Figure 2, Table 5).

The ^{1}H-NMR spectrum showed two typical pyrazine core signals at δ_H ~8.2 ppm and δ_H ~7.8 ppm with multiplicity and coupling constants corresponding to one proton at positions 5 and 6, respectively.

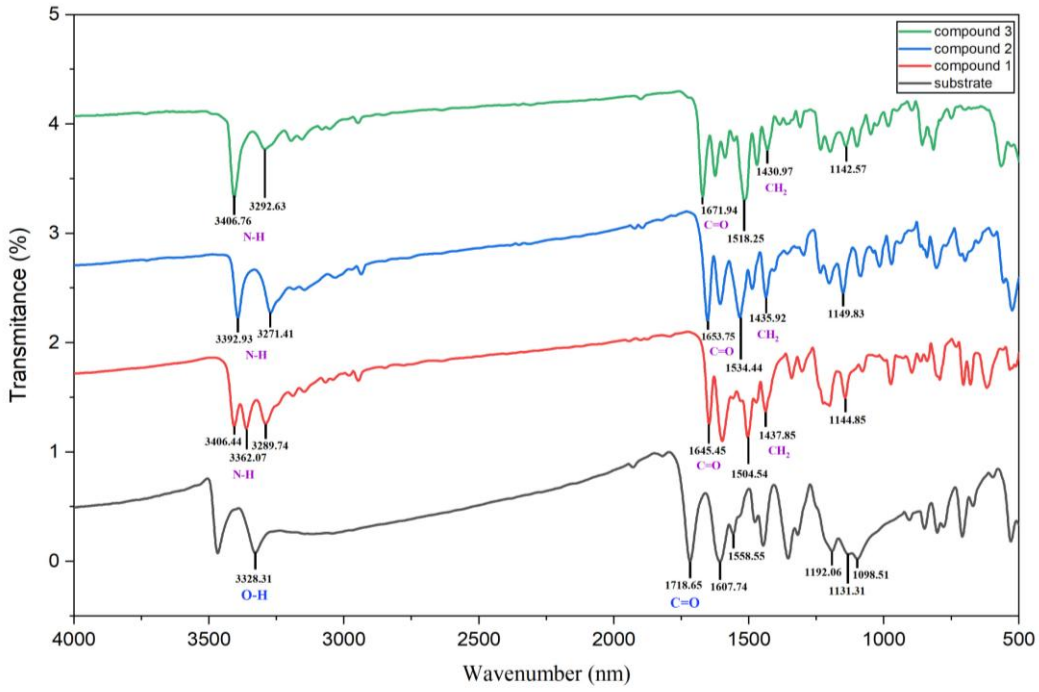

Figure 2. Comparison FT-IR spectrum of compounds **1–3** with substrate

Table 5. Interpretation of FT-IR spectrum

Substrate	Compound 1	Compound 2	Compound 3	Interpretation
1,098.51 1,131.31	1,144.85	1,149.83	1,142.57	C-N amine/amide
1,607.74	1,504.54	1,534.44	1,518.25	C=C aromatic
1,718.65	-	-	-	C=O carboxylic acid
-	1,645.45	1,653.75	1,671.94	C=O amide
-	1,437.85	1,435.92	1,430.97	CH_2 (Bend)
1,558.55 (bend)	3,406.44 3,362.07 3,289.74 (Stretch)	3,392.93 3,271.41 (Stretch)	3,292.63 3,406.76 (Stretch)	N-H Amine/Amide
3,328.31	-	-	-	O-H carboxylic acid

A broad singlet signal at δ_H ~7.5 ppm indicated the presence of an amine group at position 3. The amide proton (-NH-) was indicated by a triplet signal at δ_H ~9.3 ppm. The methylene proton was indicated by a signal at δ_H ~4.4 ppm. The difference in the ^{1}H-NMR spectra between compounds 1, 2, and 3 lies in the aromatic proton signal. The aromatic proton signal of compounds 1 and 2 appeared at δ_H ~7 ppm, with the same integration indicating the presence of four protons, but with different multiplicity patterns (Table 6). Meanwhile, the spectrum of compound 3 revealed only three aromatic signals with corresponding multiplicities and coupling constants for the 3', 5', and 6' positions (Table 6).

The ^{13}C-NMR spectra of compounds **1–3** each indicated the presence of 12 carbons. The amide carbonyl signal appeared at δ_C ~ 166 ppm, while the methylene carbon signal appeared at δ_C ~ 41 ppm for compounds **1** and **2**, and at δ_C ~ 60 ppm for compound **3**. Compound **3** has two chlorine substituents as withdrawing groups. An additional chlorine group at ortho position toward the methylene is suggested to provide a greater deshielding effect on the methylene in compounds **1** and **2**. Moreover, the methylene carbon of compound **3** bonded to the nitrogen atom can appear in the chemical shift region around 55–65 ppm [35]. The other 10 carbon signals indicated four aromatic carbons from the pyrazine ring and six aromatic carbons from the benzylamine ring (Table 6)

The structures of compounds **1-3** were further confirmed through 2D NMR measurements to determine proton-carbon single bond correlation (HSQC) and correlations between carbons and protons separated by two, three, and four bonds (HMBC). In this study, 2D NMR measurements were performed on compound **2**, which represents compounds **1–3** HSQC and HMBC were used to prove the correlation between molecular parts, specifically the correlation between the pyrazine nucleus, the methylene group (CH_2), and the benzyl ring. In the three synthesized compounds, this main framework did not undergo any changes, as the differences between the compounds were only in the position of the substituents on the benzyl ring. Therefore, the 2D NMR correlations obtained in one compound can be considered representative of the correlation

patterns in all compounds with the same core framework. The difference in substituent position between compounds can be clearly distinguished through the ^{1}H-NMR and ^{13}C-NMR spectra without the need to repeat the same 2D NMR data [36]. Based on the HMBC and HSQC spectra, the correlations that occurred in the synthesized compounds were consistent. The correlation of protons and carbon in compound **2** based on the HMBC and HSQC spectra is shown in Figure 3 and Supplementay Information. The high-resolution mass spectra (HRMS) (Table 7) of compounds **1** and **2** showed a molecular ion peak $[M+H]^+$ at m/z 263.0693, with a theoretical calculation of 263.0700.

Table 6. Interpretation of ^{1}H-NMR and ^{13}C-NMR spectrum

H/C	Chemical shift (ppm)					
	Compound 1		Compound 2		Compound 3	
	δ_H	δ_C	δ_H	δ_C	δ_H	δ_C
2	-	127.2	-	125.6	-	127.4
3	-	155.2	-	155.2	-	155.2
5	8.22 (*d*, *J*= 2.3)	147.0	8.21 (*d*, *J*= 2,35)	146.9	8.24 (*d*, *J*= 2,35)	147.2
6	7.84 (*d*, *J*= 2.3)	131.0	7.83 (*d*, *J*= 2,3)	131.3	7.86 (*d*, *J*= 2,3)	135.6
-CO-	-	166.2	-	166.1	-	166.3
-NH-	9.38 (*t*, *J*= 6.35)	-	9.36 (*t*, *J*= 6.35)	-	9.34 (*t*, *J*= 6.35)	-
-CH_2-	4.44 (*d*, *J*= 6.4)	41.7	4.42 (*d*, *J*= 6,4)	41.5	4.49 (*d*, *J*= 6,25)	60.5
1’	-	142.2	-	131.0	-	132.7
2’	7.36 (*t*, *J*= 2.0)	130.2	7.35 (*dd*, *J*= 8.7, 20.6)	128.2	-	131.1
3’	-	132.9	7.35 (*dd*, *J*= 8.7, 20.6)	129.2	7.60 (*d*, *J*= 2.1)	129.7
4’	7.28 (*t*, *J*= 7.9)	126.1	-	138.6	-	132.1
5’	7.28 (*t*, *J*= 7.9)	125.6	7.35 (*dd*, *J*= 8.7, 20.6)	129.2	7.39 (*dd*, *J*= 8.35; 2,1)	125.4
6’	7.33 (*d*, *J*= 7.7)	127.2	7.35 (*dd*, *J*= 8.7, 20.6)	128.2	7.30 (*d*, *J*= 8,35)	128.5
-NH_2	7.52 (*bs*)	-	7.54 (bs)	-	7.48 (*bs*)	-

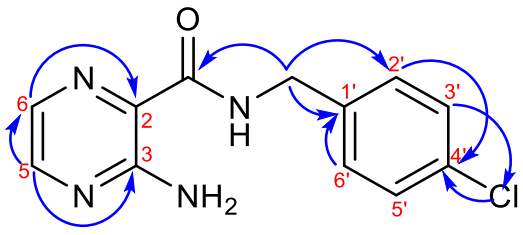

2

Figure 3. Proton and carbon correlation of **2** based on HMBC and HSQC spectra

Table 7. Interpretation of HRMS spectrum

Compound	m/z $[M+H]^+$	Calc. mass	m/z $[M+H+2]^+$	Molecular formula
1	263.0693	263.0700	265.0811	$C_{12}H_{11}N_4OCl$
2	263.0693	263.0700	265.0811	$C_{12}H_{11}N_4OCl$
3	297.0309	297.0310	299,0343	$C_{12}H_{10}N_4OCl_2$

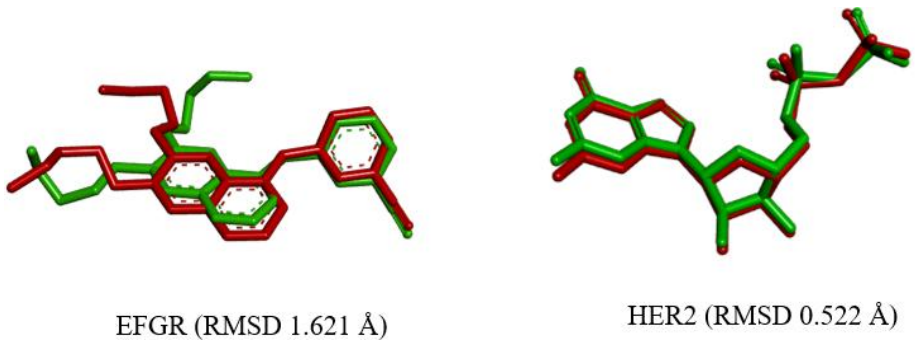

Figure 4. Visualization of docking method validation on EGFR and HER2

Compounds **1** and **2** have the same molecular formula but differ in the position of the Cl group (positional isomers), so they have an identical molecular formula and produce the same m/z value [37]. This result is valid and indicates that the molecular formula of compounds **1** and **2** is $C_{12}H_{11}N_4OCl$. The measurement results for compound **3** showed a molecular ion peak $[M+H]^+$ at m/z 297.0309 with a theoretical calculation of 297.0310, indicating that the molecular formula of compound **3** is $C_{12}H_{10}N_4OCl_2$. The presence of chloride groups in all three compounds is confirmed by the appearance of the $[M+H+2]^+$ peak with a 1:3 ratio to the molecular ion peak.

The inhibitory potential of compounds **1–3** against HER2 and EGFR was studied *in silico* using molecular docking, and their pharmacological effects and toxicity were estimated. The validation results of the ligand docking method against EGFR and HER2 were declared valid, as indicated by the root mean square deviation (RMSD) value lower than 2 Å, and showed a clear overlap between the conformations of the redocked ligand and the original ligand (Figure 4).

Molecular docking results suggest that among compounds **1–3**, compound **1** shows the most favorable predicted interaction with EGFR, indicating its potential as a candidate EGFR inhibitor (Table 8). Compound **1** is predicted to form hydrogen bonds with the key residues Glu738, Thr830, and Asp831 with a hydrogen bond distance above 1.85 Å (Figure 5), thus categorizing it as a weak to moderate hydrogen interaction. Compared with Erlotinib, the number of hydrogen interactions in compound **1** was predicted to be higher (Table 9). A higher number of hydrogen bonds contributes to a more stable ligand orientation in the active pocket, strengthening the stability of the ligand-receptor complex and increasing inhibitory potential [38].

Compound **1** is also thought to interact with key residues Thr766 (gatekeeper) and Met769 (hinge). The interaction between these two residues is crucial because the gatekeeper and hinge residues are known to be binding anchor points for first-generation EGFR inhibitors [39]. This suggests that the test ligand is expected to occupy the appropriate position inside the ATP binding pocket and replicate the interaction pattern of the previously validated inhibitor pharmacophore. Compound **3** had the most favorable predicted interaction with HER2 (Table 8) and is expected to establish a hydrogen bond with Thr862 (Figure 5).

Table 8. Docking results of ligands with EGFRand HER2

Ligand	Affinity (kkal/mol)	
	EGFR	HER2
Control (Erlotinib)	-7.3	-9.3
Compound **1**	**-**7.4	**-**8.6
Compound **2**	-6.8	**-**8.6
Compound **3**	-7.1	-9.0

Table 9. Protein-ligand interaction

Ligand	Interaction	Amino acid residues	
		EGFR	HER2
Native	*Hydrogen Bond*	**Met769***	Met801, **Asp863***
	Van Der Waals	Gly695, Val702, Glu738, Met742, **Thr766***, Leu768, Pro770, Phe771, Gly772, and Asp831	Ile752, Ala771, Ser783, Val797, **Thr798***, Leu800, Gly804, **Cys805***, and Arg849
	Carbon and Pi-Donor Hydrogen Bond	Gln767and Thr830	Gly729, Gln799, Asn850, and Thr862
Erlotinib (Control)	*Hydrogen Bond*	**Met769***	**Asp863***
	Van Der Waals	Gly695, Phe699, Met742, **Thr766***, Gln767, Leu768, Phe771, Thr830, and Asp831	Leu726, Ser728, Gly729, Ile752, Ile767, Glu770, Leu800, Gly8004, **Cys805***, Arg849, Asn850, Leu852, Leu796, Met801, Arg849, and Thr862
	Carbon and Pi-Donor Hydrogen Bond	Leu694, Pro770, and Gly772	
Compound **1**	*Hydrogen Bond*	Glu738, Thr830, Asp831	
	Van Der Waals	Val702, Met742, Leu764, **Thr766***, Leu768, **Met769***, Gly772, and Phe832	Gly729, Ala751, Glu770, Ala771, Ser783, **Thr798***, and Asp863
	Carbon and Pi-Donor Hydrogen Bond		
Compound **2**	*Hydrogen Bond*	Lys721and Thr830	Thr862 and **Asp863***,
	Van Der Waals	Leu764, **Thr766***, Gly772, Asp831, and Phe832	Lys753, Met774, Arg784, and Leu796
	Carbon and Pi-Donor Hydrogen Bond		Ser783, and **Thr798***
Compound **3**	*Hydrogen Bond*	Glu738, Met742, Thr830	Thr862
	Van Der Waals	Gly772, **Met769***, and Asp831	Gly729, Lys753, Glu770, Arg784, Leu796**, Asp863***, and **Thr798***
	Carbon and Pi-Donor Hydrogen Bond	Ala719, Leu764, and **Thr766***	Ser783

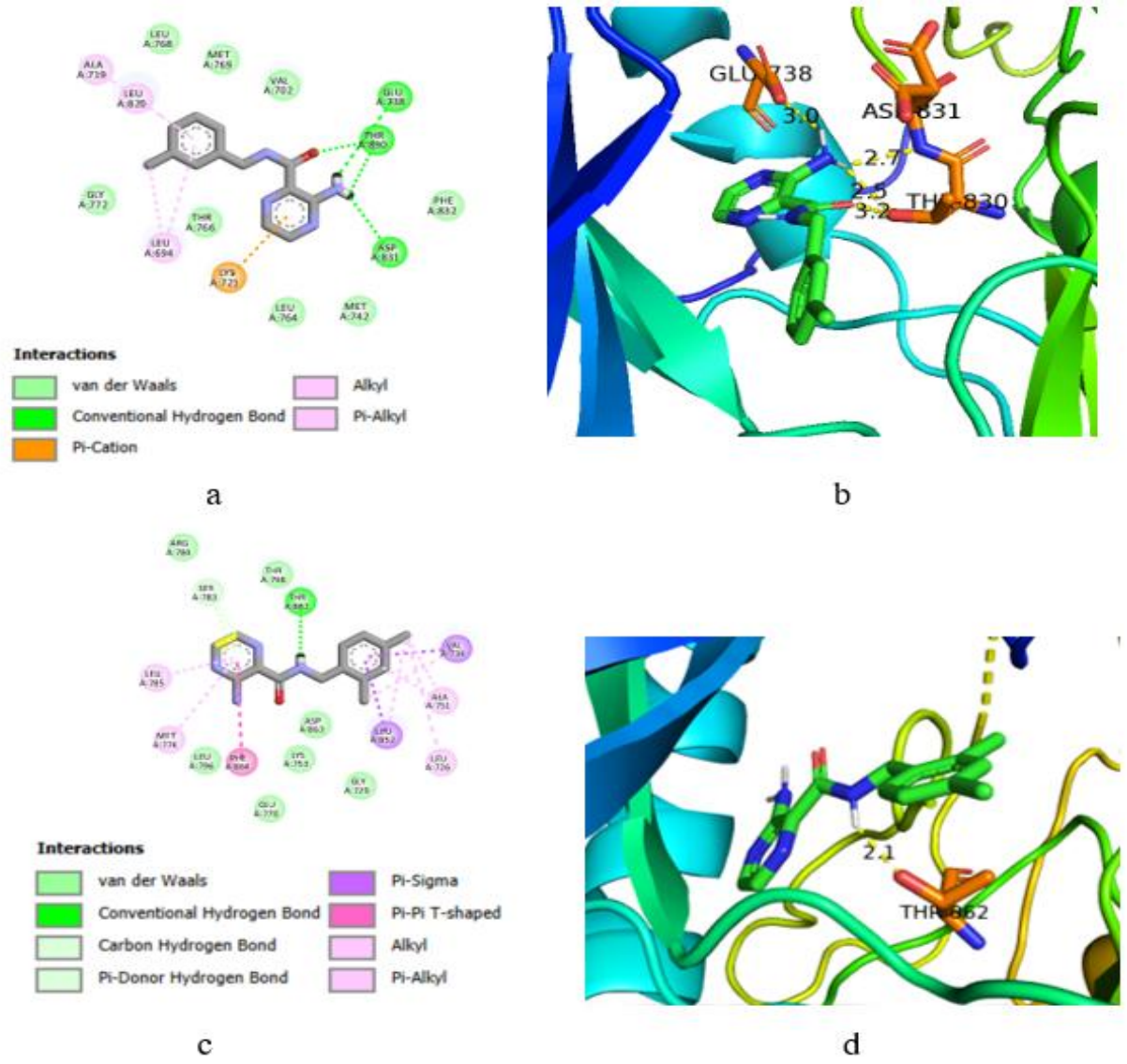

Figure 5. 2D and 3D visualization of compound **1**-EGFR interaction (a, b) and compound **3**-HER2 interaction (c, d)

In the HER2 domain, the catalytic residues are located around the HRD/DFG motif (including Asp863). The position of Thr862, which is adjacent to Asp863 in the DFG motif, suggests that compound **3** occupies the region around the HER2 catalytic domain. Furthermore, compound 3 is alleged to have hydrophobic interactions with Thr798 as a gatekeeper that regulates ligand access to the ATP pocket [40] (Table 9). Compared to Erlotinib, which forms a hydrogen bond with Asp863 and only interacts with Thr862 through van der Waals forces, compound **3** forms a direct hydrogen bond with Thr862 and interacts hydrophobically with Asp863 (Table 9). This difference in interaction patterns predicts that compound **3** and Erlotinib both occupy the ATP-binding pocket, but with slightly different orientations around the Thr862–Asp863 residue pair. The interactions predicted through this molecular docking study represent an initial screening, indicating the potential of compounds **1–3** as a preliminary lead for EGFR and HER2 inhibitors. This *in silic*o study requires further *in vitro* and *in vivo* assays to validate its biological relevance.

Table 10. ADME and toxicity prediction

Compound	*Lipinski's rule of five*						TPSA (Å²)	MSA	LD_{50} (mg/kg)	Toxicity class
	MW (g/mol)	RB	HBA	HBD	LogP	Violations				
Erlotinib	393.44	10	6	1	3.67	0	74.73	3.19	125	3
1	262.69	4	3	2	1.49	0	80.90	2.05	1,000	4
2	262.69	4	3	2	1.45	0	80.90	2.00	1,000	4
3	297.14	4	3	2	2.08	0	80.90	2.17	1,000	4

MW: molecular weight, RB: number of Rotatable bonds, HBA: number of Hydrogen Bonds Acceptor, HBD: number of Hydrogen Bonds Donor, Log P: Lipophilicity, TPSA: Topological Polar Surface area, and MSA: Medicinal Synthesis Accessibility.

The molecular docking results presented in this paper provide a basic overview of protein-ligand interactions, including static binding sites. The desolvation energy and entropic effects are not explicitly captured by the docking scoring functions used in this study. There were no molecular dynamics simulations performed; therefore, the long-term reliability of the interactions under physiological settings cannot be investigated, which is a limitation of this research. The presented interactions correspond to reasonable docking predictions, and more molecular dynamics studies are required to verify binding stability.

Pharmacokinetic, toxicity, and drug-likeness predictions (Table 10) indicate that Erlotinib and compounds **1**–**3** fulfill Lipinski and Veber's rules. Like Erlotinib, compounds **1**–**3** have log P < 5 and TPSA ≤ 140 Å², thus predicted to have the ability to penetrate lipid membranes passively and are suitable for oral absorption [41]. All three compounds are classified as class 4 toxicity, with LD_{50} values of 1,000 mg/kg, while Erlotinib is classified as class 3, with an LD_{50} value of 125 mg/kg [42]. The toxicity classifications presented in ProTox-II are *in silico* predictions rather than direct correlations to the toxicological effects of compounds. This result depends on the machine learning models and their specific application areas. Compounds in the same toxicity class in ProTox-II may not have comparable predictive power. ADME and toxicology predictions represent only screening-level computational estimates and should be interpreted as preliminary computational indicators, not confirmed safety profiles.

Conclusion

The synthesis of three chlorinated benzylamine-substituted pyrazine derivatives has been successfully carried out using CDI catalysts in a one-pot reaction. The molecular structures of the three compounds have been comprehensively determined through FT-IR, ^{1}H-NMR, ^{13}C-NMR, HMBC, HSQC, and HRMS spectra. MAS proved superior to conventional and UAS methods because it is faster, energy-efficient, and produces higher yields. The one-pot process also reduces intermediate purification, thus saving solvents and generating less waste. Among the three compounds, compound **1** is predicted to be more favorable as an EGFR inhibitor, while compound **3** is more favorable as an HER2 inhibitor. Predicted pharmacokinetics, toxicity, and drug-likeness provide a good initial safety prediction for compounds **1**–**3** but must be followed up with experimental toxicology to confirm the safety issues. The three compounds can be recommended for further evaluation *in vitro* and *in vivo* as anticancer candidates based on EGFR and HER2 inhibitors.

Acknowledgement

The authors would like to express their sincere gratitude to the Directorate of Research and Community Service, Directorate General of Research and Development of the Ministry of Higher Education, Science and Technology for the research funding provided in the 2025 fiscal year through the REGULAR FUNDAMENTAL RESEARCH scheme with contract number: 105/C3/DT.05.00/PL/2025 and the research assignment agreement letter number of LPPM UNS: 1186.1/UN27.22/PT.01.03/2025.

Disclosure Statement

No potential conflict of interest was reported by the authors.

ORCID

Widiastuti Agustina Eko Setyowati:
https://orcid.org/0000-0002-7261-623X
Imarotul Unsiyah:
https://orcid.org/0009-0007-1176-5657
Celicarina Anwar:
https://orcid.org/0009-0000-5551-5982
Muhammad Hizbul Wathon:
https://orcid.org/0000-0002-7580-1641
Elfi Susanti VH:
https://orcid.org/0000-0001-9243-5623
Sri Retno Dwi Ariani:
https://orcid.org/0000-0002-3431-4679

References

[1] Hou, W., Dai, W., Huang, H., Liu, S.-L., Liu, J., Huang, L.-J., Huang, X.-H., Zeng, J.-L., Gan, Z.-W., Zhang, Z.-Y. Pharmacological activity and mechanism of pyrazines. *European Journal of Medicinal Chemistry*, **2023**, 258, 115544.

[2] Chen, G.-Q., Guo, H.-Y., Quan, Z.-S., Shen, Q.-K., Li, X., Luan, T. Natural products–pyrazine hybrids: A review of developments in medicinal chemistry. *Molecules*, **2023**, 28(21), 7440.

[3] Liu, X., Li, Y., Zhang, Q., Pan, Q., Zheng, P., Dai, X., Bai, Z., Zhu, W. Design, synthesis, and biological evaluation of [1, 2, 4] triazolo [4, 3-a] pyrazine derivatives as novel dual c-met/vegfr-2 inhibitors. *Frontiers in Chemistry*, **2022**, 10, 815534.

[4] Zhang, B., Liu, X., Xiong, H., Zhang, Q., Sun, X., Yang, Z., Xu, S., Zheng, P., Zhu, W. Discovery of [1, 2, 4] triazolo [4, 3-*a*] pyrazine derivatives bearing a 4-oxo-pyridazinone moiety as potential c-met kinase inhibitors. *New Journal of Chemistry*, **2020**, 44(21), 9053-9063.

[5] Setyowati, W.A.E., Syah, Y.M., Ihsanawatia, A.A. Chemical transformation of pyrazine derivatives. *Moroccan Journal of Chemistry*, **2022**, 10(2), 2288-2297.

[6] Setyowati, W.A.E., Ihsanawati, I., Alni, A. Optimization of nitration of 3-hydroxypyrazine-2-carboxamide to 3-hydroxy-6-nitropyrazine-2-carboxamide. *JKPK (Jurnal Kimia dan Pendidikan Kimia)*, **2023**, 8(3), 384-395.

[7] Sivaiah,, G., Raveesha, R., Prasad, S.B., Kumar, K.Y., Raghu, M., Alharethy, F., Prashanth, M., Jeon, B.-H. Synthesis, anticancer activity and molecular docking of new pyrazolo [1, 5-a] pyrimidine derivatives as egfr/her2 dual kinase inhibitors. *Journal of Molecular Structure*, **2023**, 1289, 135877.

[8] Benedetto Tiz, D., Bagnoli, L., Rosati, O., Marini, F., Sancineto, L., Santi, C. New halogen-containing drugs approved by FDA in 2021: An overview on their syntheses and pharmaceutical use. *Molecules*, **2022**, 27(5), 1643.

[9] Gai, C., Zhang, Y., Zhang, S., Hu, X., Song, Y.-Q., Zhuang, X., Chai, X., Zou, Y., Ge, G.-B., Zhao, Q. The study of halogen effect on the reactivity of the serine-targeting covalent warheads. *Frontiers in Chemistry*, **2024**, 12, 1504453.

[10] Roskoski Jr, R. Properties of fda-approved small molecule protein kinase inhibitors: A 2024 update. *Pharmacological Research*, **2024**, 200, 107059.

[11] Setyowati, W.A.E., Hermawati, E., Ihsanawati, Alni. A. Synthesis, characterization, tyrosine kinase inhibitory studies, and molecular docking analysis of pyrazine-2-carboxamide derivatives. *Advanced Journal of Chemistry Section A*, **2025**, 8, 2098–2112.

[12] Vijayarathinam, M., Kannan, A., Akilan, P., Chandrasekaran, V., Gunasekaran, T. A novel approach in the synthesis of indoloquinoline alkaloid analogues: Spectroscopic and DFT exploration, molecular docking of COVID-19 and ADMET properties. *Advanced Journal of Chemistry Section A,* **2024**, 7, 417–437.

[13] Trott, O., Olson, A.J. Autodock vina: Improving the speed and accuracy of docking with a new scoring function, efficient optimization, and multithreading. *Journal of Computational Chemistry*, **2010**, 31(2), 455-461.

[14] Ziaie, Z.M., Mokhtary, M. A theoretical investigation of heterocycles with N–O bonds understanding the biological effects and theoretical

studies: From theory to applicatio. *Journal of Chemical Reviews*, **2025**, 7(2), 166-190.
[15] Ayodele, P.F., Bamigbade, A., Bamigbade, O.O., Adeniyi, I.A., Tachin, E.S., Seweje, A.J., Farohunbi, S.T. Illustrated procedure to perform molecular docking using pyrx and biovia discovery studio visualizer: A case study of 10kt with atropine. *Progress in Drug Discovery & Biomedical Science*, **2023**, 6(1).
[16] Cai, H., Liao, S., Li, J., Lv, M., Lin, X., Song, Y., Chen, X., Zhu, Y., Zhang, J., Qi, N. Structure-based virtual screening of potential inhibitors targeting the prolyl-tRNA synthetase (PRS) in *Eimeria tenella*: Insights from molecular docking, admet studies, and molecular dynamics simulations. *Molecules*, **2025**, 30(4), 790.
[17]. Rosignoli, S., Paiardini, A. Boosting the full potential of pymol with structural biology plugins. *Biomolecules*, **2022**, 12(12), 1764.
[18] Stamos, J., Sliwkowski, M.X., Eigenbrot, C. Structure of the epidermal growth factor receptor kinase domain alone and in complex with a 4-anilinoquinazoline inhibitor. *Journal of Biological Chemistry*, **2002**, 277(48), 46265-46272.
[19] Aertgeerts, K., Skene, R., Yano, J., Sang, B.-C., Zou, H., Snell, G., Jennings, A., Iwamoto, K., Habuka, N., Hirokawa, A. Structural analysis of the mechanism of inhibition and allosteric activation of the kinase domain of her2 protein. *Journal of Biological Chemistry*, **2011**, 286(21), 18756-18765.
[20] Bouz, G., Semelková, L., Janďourek, O., Konečná, K., Paterová, P., Navrátilová, L., Kubíček, V., Kuneš, J., Doležal, M., Zitko, J. Derivatives of 3-aminopyrazine-2-carboxamides: Synthesis, antimicrobial evaluation, and in vitro cytotoxicity. *Molecules*, **2019**, 24(7), 1212.
[21] Valeur, E., Bradley, M. Amide bond formation: Beyond the myth of coupling reagents. *Chemical Society Reviews*, **2009**, 38(2), 606-631.
[22] Hayashi, Y. Pot economy and one-pot synthesis. *Chemical Science*, **2016**, 7(2), 866-880.
[23] Mutungi, M.M., Ho, C.C., Bissember, A.C., Smith, J.A. Facilitating the isolation of polar natural products: Mild 1, 1′-carbonyldiimidazole-enabled method for derivatization of acids and alcohols. *European Journal of Organic Chemistry*, **2025**, 28(28), e202500231.
[24] Kwon, K., Simons, R.T., Nandakumar, M., Roizen, J.L. Strategies to generate nitrogen-centered radicals that may rely on photoredox catalysis: Development in reaction methodology and applications in organic synthesis. *Chemical Reviews*, **2021**, 122(2), 2353-2428.
[25] Bansagi, J., Wilson-Konderka, C., Debrauwer, V., Narayanan, P., Batey, R.A. N-alkyl carbamoylimidazoles as isocyanate equivalents: Exploration of the reaction scope for the synthesis of ureas, hydantoins, carbamates, thiocarbamates, and oxazolidinones. *The Journal of Organic Chemistry*, **2022**, 87(17), 11329-11349.
[26] Frecentese, F., Sodano, F., Corvino, A., Schiano, M.E., Magli, E., Albrizio, S., Sparaco, R., Andreozzi, G., Nieddu, M., Rimoli, M.G. The application of microwaves, ultrasounds, and their combination in the synthesis of nitrogen-containing bicyclic heterocycles. *International Journal of Molecular Sciences*, **2023**, 24(13), 10722.
[27] Baig, R.N., Varma, R.S. Alternative energy input: Mechanochemical, microwave and ultrasound-assisted organic synthesis. *Chemical Society Reviews*, **2012**, 41(4), 1559-1584.
[28] Ghosh, A., Patil, G., Patel, P., Basak, S., Saxena, K.K., Tyagi, R., sunil, B.D.Y., Khan, M.I., Dubey, K.K., Lakshmi, A.A. A review on mxenes and its various potential synthesis strategies. *Journal of Chemical Reviews*, **2025**, 7(3), 381-420.
[29] Camargo, D., Cifuentes, C., Castillo, J.-C., Portilla, J. Microwave-assisted synthesis and functionalization of 2-arylimidazo [1,2-*a*] pyrimidin-5 (8*H*)-ones. *RSC Advances*, **2024**, 14(31), 22368-22373.
[30] Chakraborty, A., Giri, S., Adhikari, T. Microwave assisted synthesis: An eco-friendly green chemistry approach of drug synthesis. *International Journal of Pharmacy and Pharmaceutical Sciences*, **2024**, 6, 149–156.
[31] Schneider, H., Merbouh, N., Keerthisinghe, S., Antonietti, M., Filonenko, S. Microwave-irradiated rapid synthesis of antimicrobial pyrazine derivatives in reactive eutectic media. *Green Chemistry*, **2022**, 24(24), 9745-9754.
[32] Elie, J., Fruit, C., Besson, T. Microwave-assisted sequential one-pot synthesis of 8-substituted pyrazolo [1, 5-*a*] [1, 3, 5] triazines. *Molecules*, **2021**, 26(12), 3540.
[33] Sajini, T., Joseph, J. Microwave-assisted synthesis of nanomaterials: A green chemistry perspective and sustainability assessment. *RSC Sustainability*, **2025**, 3(11), 4911-4935.
[34] Rajkumar, P., Selvaraj, S., Anthoniammal, P., Kumar, A.R., Kasthuri, K., Kumaresan, S. Structural (monomer and dimer), spectroscopic (FT-IR, FT-Raman, UV–Vis and NMR) and solvent effect (polar and nonpolar) studies of 2-methoxy-4-vinyl phenol. *Chemical Physics Impact*, **2023**, 7, 100257.
[35] Viesser, R.V., Ducati, L.C., Tormena, C.F., Autschbach, J. The halogen effect on the 13 C NMR chemical shift in substituted benzenes. *Physical Chemistry Chemical Physics*, **2018**, 20(16), 11247-11259.

[36] Claridge, T.D. High-resolution nmr techniques in organic chemistry. *High-resolution NMR Techniques in Organic Chemistry*, **2016**, 27.
[37] Gross, J.H. Mass spectrometry: A textbook. **2006**.
[38] Derewenda, Z.S., Hawro, I., Derewenda, U. C— H··· O hydrogen bonds in kinase-inhibitor interfaces. *IUBMB Life,* **2020**, 72, 1–10.
[39] Du, Y., Karatekin, F., Wang, W.K., Hong, W., Boopathy, G.T. Cracking the egfr code: Cancer biology, resistance mechanisms, and future therapeutic frontiers. *Pharmacological Reviews*, **2025**, 100076.
[40] Yu, X., Wang, T., Lou, Y., Li, Y. Combination of in silico analysis and in vitro assay to investigate drug response to human epidermal growth factor receptor 2 mutations in lung cancer. *Molecular Informatics*, **2016**, 35(1), 25-35.
[41] Fernandes, J., Gattass, C.R. Topological polar surface area defines substrate transport by multidrug resistance associated protein 1 (MRP1/ABCC1). *Journal of Medicinal Chemistry*, **2009**, 52(4), 1214-1218.
[42] Gadaleta, D., Vuković, K., Toma, C., Lavado, G.J., Karmaus, A.L., Mansouri, K., Kleinstreuer, N.C., Benfenati, E., Roncaglioni, A. SAR and QSAR modeling of a large collection of LD50 rat acute oral toxicity data. *Journal of Cheminformatics*, **2019**, 11(1), 58.

HOW TO CITE THIS ARTICLE

W.A.E. Setyowati, I. Unsiyah, C. Anwar, M.H. Wathon, E.S. VH, S.R.D. Ariani. One-Pot Microwave-Assisted Synthesis of Chlorinated Benzylamine-Substituted Pyrazine Derivatives and *In Silico* Studies of Their Potential as EGFR and HER2 Inhibitors. *Adv. J. Chem. A*, 2026, 9(7), 1242-1257.

DOI: 10.48309/AJCA.2026.565862.2000
URL: https://www.ajchem-a.com/article_240497.html